Available online at www.sciencedirect.com
ScienceDirect
Journal of Solid State Chemistry 180 (2007) 265–275
JOURNAL OF SOLID STATE CHEMISTRY
www.elsevier.com/locate/jssc

Structural characterization, thermal and electric properties of imidazolium bromoantimonate(III): $[C_3H_5N_2]_3[Sb_2Br_9]$

A. Piecha, V. Kinzhybalo, K. Ślepokura, R. Jakubas*

Faculty of Chemistry, University of Wrocław, Joliot–Curie 14, 50–383 Wrocław, Poland

Received 11 July 2006; received in revised form 14 October 2006; accepted 16 October 2006
Available online 21 October 2006

Abstract

Tris(imidazolium) nonabromodiantimonate(III), $[C_3H_5N_2]_3[Sb_2Br_9]$, is trimorphic. Its crystal structure has been determined at 100 K (form I) and 293 K (form II) by X-ray single crystal diffraction in, respectively, the monoclinic space groups, $P2_1/c$ (form I) and $P2_1/n$ (form II). In both structures, the anionic sublattice forms corrugated two-dimensional layers in the *bc* plane. In forms I and II there are, respectively, three and two crystallographically independent imidazolium cations. Two types of cations are present in the structures: the one that occupies cavities within the polyanions layer appears to be ordered in the lowest temperature form I and disordered in form II. The second type of imidazolium cations placed between the layers is ordered over the studied temperature region. The temperature dependence of the lattice parameters has been determined between 100 and 280 K. DSC studies indicate a presence of two reversible phase transitions: continuous at 237 K (I → II) and discontinuous at 373/351 K (heating–cooling) from form II to form III. The phase transition II → III is accompanied by a huge entropy transition ($\Delta S_{II\to III}$) equal to ca. 28 $Jmol^{-1}K^{-1}$, which suggests an order (form II)–disorder (form III) transition mechanism. The dielectric relaxation process was found to appear in a low frequency region over the form I with an activation energy ca. 16.5 kJ/mol. A polydispersive character of the dielectric dispersion indicates a presence of complex molecular motions of dipolar groups in the title compound. The explanation of mechanism of the I → II phase transition in $[C_3H_5N_2]_3[Sb_2Br_9]$ is proposed.

PACS: 72.22.Gm; 61.10.−i; 64.70.Kb

Keywords: Halogenoantimonates(III); Imidazolium cation; Phase transition; Dielectric relaxation

1. Introduction

A characteristic feature of molecular-ionic halogenoantimonates(III) and halogenobismuthates(III) described by the general formula $R_aM_bX_{(3b+a)}$ (where *R* denotes organic cation, *M* denotes Sb(III) or Bi(III) and *X* = Cl, Br, I), is a rich diversity of the anionic sublattice. More than 30 various anionic structures have been isolated so far [1–3]. Numerous experimental studies showed that the structure of the anionic sublattice is frequently related to the size and symmetry of the cations and halogen atoms as well. The organic cations embedded in the inorganic sublattice are dynamically disordered. The releasing of motion of dipolar cations, in some cases, may lead to a long-range dipole–dipole order of ferroelectric type. It is interesting that ferroelectric properties were observed only in salts with the stoichiometry of $R_3M_2X_9$ [4,5] and $R_5M_2X_{11}$ [6–9]. Many reports have been devoted to the crystals with the $R_3M_2X_9$ composition, which are characterized by three terminal halogen atoms and three bridging ones [10–13]. The $[MX_6]$ octahedra can form either infinite one-dimensional chains [14], two-dimensional layers and discrete bioctahedral [3] or four-octahedral units $(M_4X_{18})^{6-}$ as well [15]. In spite of a wide variety of the anionic forms the ferroelectric properties were found to appear only in salts characterized by two-dimensional anionic layers. The cations which occupy the cavities inside the layers in the ferroelectric phase of these systems are expected to contribute to the spontaneous polarization. It was shown

*Corresponding author. Fax: +48713282228.
E-mail address: rj@wchuwr.chem.uni.wroc.pl (R. Jakubas).

0022-4596/$ - see front matter © 2006 Elsevier Inc. All rights reserved.
doi:10.1016/j.jssc.2006.10.016

that the ferroelectricity in the $R_3M_2X_9$ subgroup requires the presence of rather small and mobile counter-ions, like methyl-, dimethyl- and trimethyl-ammonium.

In the search for new polar crystals we have extended our studies on halogenoantimonates(III) and halogenobismuthates(III) embedding in the structure aromatic pentagonal cations like imidazolium. Recently, we have synthesized and studied two imidazolium chlorobismuthate(III) analogs; $[C_3N_2H_5]_6[Bi_4Cl_{18}]$ characterized by uncommon discrete $Bi_4Cl_{18}^{6-}$ anion [16] and a new ferroelectric material—$[C_3N_2H_5]_5[Bi_2Cl_{11}]$ [17].

In this paper we present the thermal and dielectric properties of tris(imidazolium) nonabromodiantimonate(III)—$[C_3H_5N_2]_3[Sb_2Br_9]$ within a wide temperature range. The structural characterization of this compound was completed at two temperatures in various forms (I and II). The mechanism of the phase transition at 237 K is studied.

2. Experimental

The starting materials were commercial $SbBr_3$ and imidazole amine ($C_3N_2H_4$). $[C_3N_2H_5]_3[Sb_2Br_9]$ crystals were prepared by dissolving stoichiometric amounts of $SbBr_3$ and imidazole in the concentrated HBr solution. The crystalline product was twice recrystallized. Single crystals were grown by slow evaporation from an aqueous solution.

Differential scanning calorimetry (DSC) runs were recorded using a Perkin Elmer DSC-7 in the temperature range 100–450 K. The dilatometric measurements were performed with a thermomechanical analyser Perkin Elmer TMA-7 in the temperature range 100–450 K. The dimensions of the crystal were of the order of $5 \times 3 \times 1\,mm^3$.

The complex electric permittivity, $\varepsilon^* = \varepsilon' - i\varepsilon''$, was measured by a HP 4285A and Agilent 4284A Precision LCR Meters in the frequency range between 1 kHz and 25 MHz and in the temperature range from 80 to 300 K. The dimensions of the sample were of the order of $5 \times 3 \times 1\,mm^3$. The overall errors in the estimation of the real and imaginary parts of the complex permittivity value were less than 5% and 10%, respectively.

The crystallographic measurements were performed on a Kuma KM4CCD automated four-circle diffractometer with the graphite-monochromatized Mo$K\alpha$ radiation. The data for the crystal were collected at 100(2) and 293(2) K using the *Oxford Cryosystems* cooler and were analytically corrected for absorption with the use of *CrysAlis RED* program [18] of the KM4CCD software, using a multifaceted crystal model based on expressions derived by Clark and Reid [19]. A summary of the conditions for the data collection and the structure refinement parameters are given in Table 1. The structures were solved by the heavy atom method using the *SHELXS*-97 program [20] and refined by the full-matrix least-squares technique using *SHELXL*-97 [20] with anisotropic thermal parameters for non-H atoms. The hydrogen atoms were treated as riding atoms and refined with N–H and C–H distances fixed (at 0.88 and 0.95 Å, respectively) and with $U_{iso}(H)$ values of $1.2U_{eq}(C)$. All imidazolium cation atoms in the crystal structure of the form II were refined as carbon atoms, whereas definite positions of nitrogen atoms were not found due to the rotational disorder.

Table 1
Experimental data for form I and II of $[C_3H_5N_2]_3[Sb_2Br_9]$

Crystal data		
Empirical formula	$C_9H_{15}Br_9N_6Sb_2$ $[C_3H_5N_2]_3[Sb_2Br_9]$	$C_9H_{15}Br_9N_6Sb_2$ $[C_3H_5N_2]_3[Sb_2Br_9]$
Formula weight ($g\,mol^{-1}$)	1169.96	1169.96
Crystal system, space group	Monoclinic, $P2_1/c$	Monoclinic, $P2_1/n$
a (Å)	20.793(4)	10.558(3)
b (Å)	8.771(2)	8.886(2)
c (Å)	15.835(3)	15.420(3)
β (°)	111.43(3)	106.98(3)
V (Å^3)	2688.3(10)	1383.6(6)
Z	4	2
D_{calc} ($g\,cm^{-3}$)	2.891	2.808
μ(mm^{-1})	15.396	14.957
F (0 0 0)	2112	1056
Crystal size (mm)	$0.10 \times 0.08 \times 0.06$	$0.30 \times 0.20 \times 0.02$
Crystal habit	Yellow-green plate	Yellow-green plate
Data collection		
Diffractometer	Kuma KM4CCD	Kuma KM4CCD
Monochromator	Graphite	Graphite
Radiation type, wavelength, λ(Å)	Mo$K\alpha$, 0.71073	Mo$K\alpha$, 0.71073
T (K)	100(2)	293(2)
Θ range (°)	3.10–27.00	3.05–27.00
Indexes range	$-20 \leqslant h \leqslant 20$ $-11 \leqslant k \leqslant 9$ $-19 \leqslant l \leqslant 19$	$-13 \leqslant h \leqslant 13$ $-10 \leqslant k \leqslant 11$ $-19 \leqslant l \leqslant 19$
Absorption correction	Analytical	Analytical
T_{min}/T_{max}	0.232/0.478	0.011/0.499
Measured reflections	31758	17486
Independent reflections	5859	3032
Observed refl. ($I > 2\sigma(I)$)	5015	2323
R_{int}	0.1045	0.2138
Refinement		
Refinement on	F^2	F^2
Data/restraints/parameters	5859/0/235	3032/0/142
$R(F_o^2 > 2\sigma(F_o^2))$	$R_1 = 0.0518$ $wR_2 = 0.0853$	$R_1 = 0.0902$ $wR_2 = 0.1979$
R (all data)	$R_1 = 0.0696$ $wR_2 = 0.0904$	$R_1 = 0.1206$ $wR_2 = 0.2173$
GooF = S	1.161	1.085
Weighting parameter a/b	0.0280/0.0	0.049/40
$\Delta\rho_{max}/\Delta\rho_{min}$ ($e\,Å^{-3}$)	0.89/ − 1.05	1.95/ − 1.08

$w = 1/[\sigma^2(F_0^2) + (aP)^2 + bP]$ where $P = (F_0^2 + 2F_c^2)/3$.

3. Results and discussion

3.1. Thermal properties

The DSC measurements were carried out over the temperature range 100–410 K. Above 410 K we observed the chemical reaction of the sample with the aluminium, therefore, the results being false were not taken into account.

The DSC curves obtained for $[C_3H_5N_2]_3[Sb_2Br_9]$ crystals upon cooling and heating scans are illustrated in Fig. 1.

Since the temperature of III → II phase transition depends on the history of the sample, therefore, several scans were carried out above room temperature (Fig. 1(a)). The first heat anomaly upon heating appears at ca. 380 K (scan 3), whereas on cooling (scan 4) it takes place at ca. 351 K. Next heating (scan 5) reveals the heat anomaly at 373 K and upon second cooling it is reversible at 351 K. The following scans lead to the sequence visible during second heating (scan 5) and cooling (scan 6). From the calorimetric measurements one can conclude that the title compound discloses two reversible phase transitions: continuous at 237 K from form I to form II and discontinuous at 373/351 K (heating–cooling) from form (II → III). The phase transition II → III is accompanied by a significant entropy transition ($\Delta S_{II\rightarrow III}$), which equals ca. 28 $Jmol^{-1}K^{-1}$. Such a value is typical for the transitions between two forms characterized by various level of disorder of two cations. The temperature hysteresis extrapolated to zero scanning rate for transition II → III was found to be 22 K.

Fig. 1(b) shows the simultaneous thermogravimetric analysis (TGA) and differential thermal analysis (DTA) scans for the $[C_3H_5N_2]_3[Sb_2Br_9]$ derivative within 300–630 K. The first large endotherm at ca. 380 K (onset at 370 K) corresponds to the structural phase transition

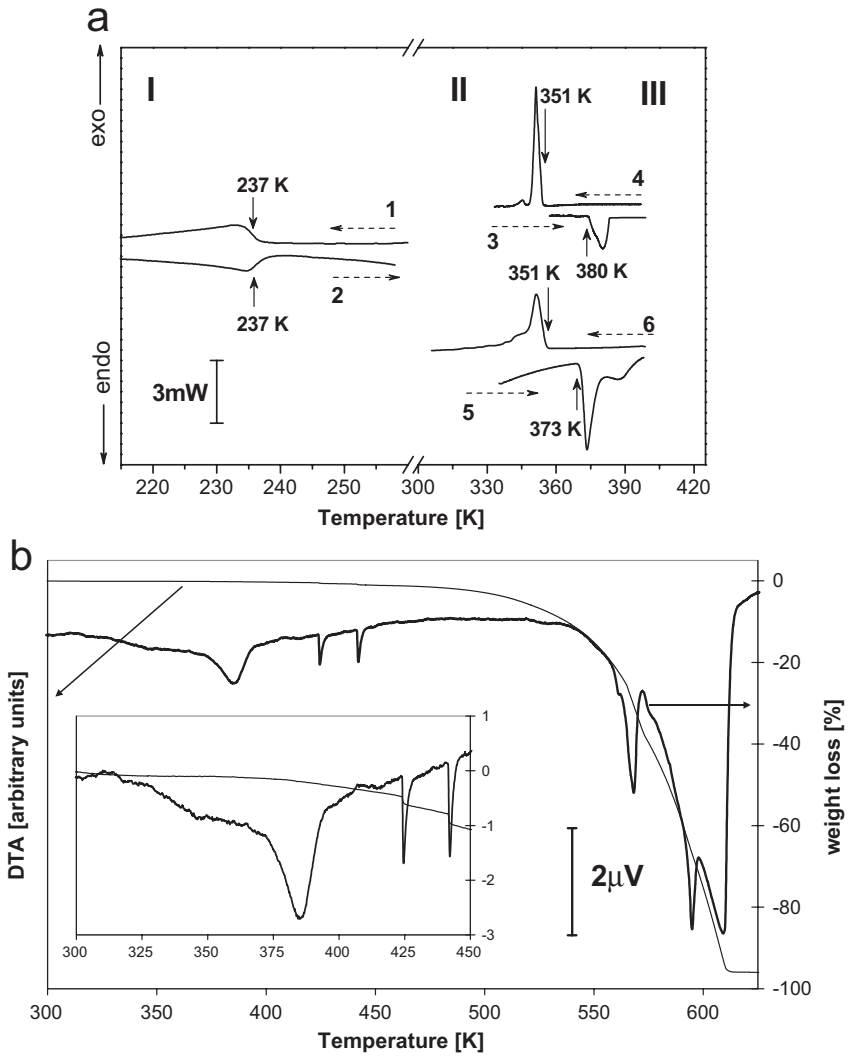

Fig. 1. (a) DSC runs for $[C_3H_5N_2]_3[Sb_2Br_9]$ at a rate of 10 K/min upon cooling and heating. Scans 1 and 2 correspond to the first cooling and heating runs, respectively, between room temperature and 100 K (for these scans only the temperature interval covering the heat anomaly is presented). (b) Simultaneous thermogravimetric analysis and differential thermal analysis scan (with the ramp rate of 2 K/min, sample mass 19.7 mg) for the $[C_3H_5N_2]_3[Sb_2Br_9]$ crystal.

detected by DSC. It is very important that it is accompanied by a negligible weight loss ca. 0.3%. The compound seems to be stable up to at least 415–420 K. Further heating leads to two sharp endotherms at ca. 420 and 440 K, which are followed by sudden but a small weight loss (the total weight loss up to 450 K is below 1%). These effects may be explained in terms of some changes on the surface of the sample. Heating above 450 K brings about a continuous and pronounced decomposition of the crystal, then above 600 K the loss of the mass sample attains 95%.

Fig. 2 shows results of the linear thermal expansion $\Delta L/L_0$, along three crystallographic axes in the vicinity of the high temperature transition obtained upon first heating. The directions presented correspond to those taken for the room temperature monoclinic symmetry. The obvious step-wise changes in the dimensions of the crystal at ca. 390 K confirm a discontinuous character of the transition. The sample expands dramatically along all directions, probably due to the swelling of the crystal. Nevertheless, for the *a*-axis just after crossing ca. 395 K a drastic contraction is visible, which reflects a real behavior of the crystal. Anomalies in dilation (not presented) upon cooling of the crystal, close to the 351 K transition temperature are only qualitatively reversible. However, the effect is markedly smaller (nearly by one order), which indicates the mechanical instability of the crystal. The sample contracts along the *c*- and *b*-axis while it expands along the *a*-direction. The optical observations show additionally that a single crystal became opaque and strongly deformed after crossing the transition temperature II → III.

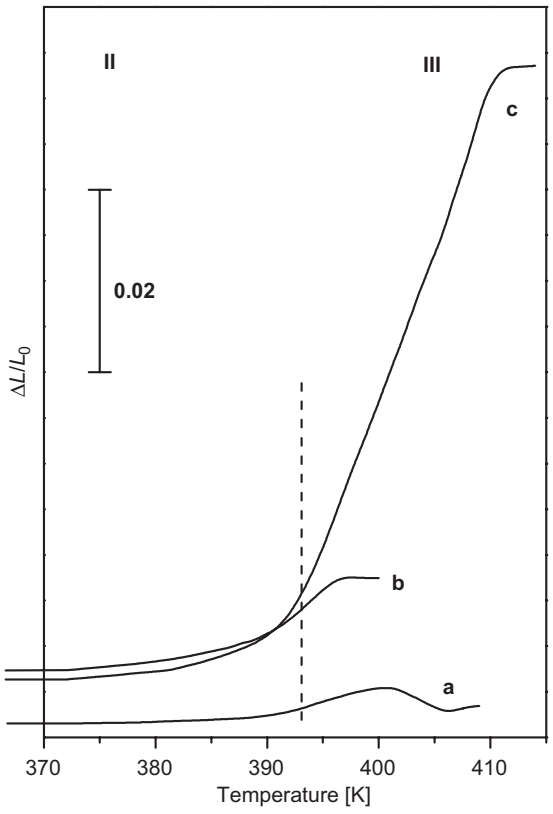

Fig. 2. The linear thermal expansion along three crystallographic axes of $[C_3H_5N_2]_3[Sb_2Br_9]$ above room temperature, upon heating.

3.2. Dielectric properties

The temperature dependence of the complex electric permittivity, ε^*, of $[C_3H_5N_2]_3[Sb_2Br_9]$ were measured along three crystallographic directions over 100–400 K for the frequencies between 0.5 kHz and 1 MHz. Fig. 3 shows the temperature dependence of ε' over the temperature region 100–280 K at several selected frequencies for two axes, *b* and *c*, upon the first cooling.

Fig. 4 presents ε'_a vs temperature and imaginary part of ε^*_a at low temperatures. The structural phase transition at 237 K is seen as a clear change in the slope of ε' vs temperature along the *c* and *a* directions and a slight jump of the permittivity for the *b* one. At low temperatures there is observed a low frequency relaxation process with the dielectric increment of ca. 2.5 and 1.5 units for the *b* and *a* axes, respectively.

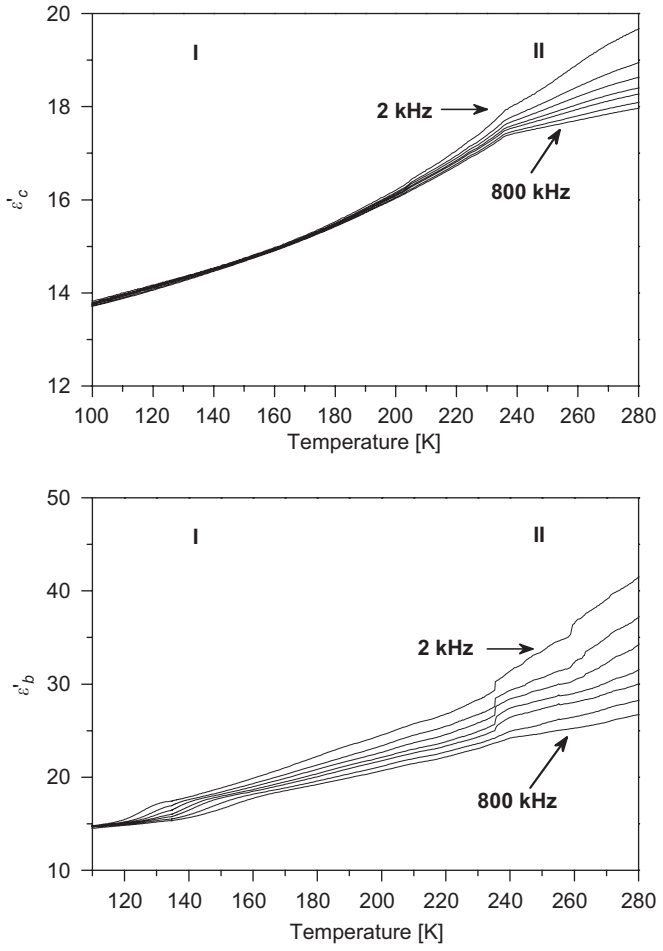

Fig. 3. The real part of complex electric permittivity, ε', at selected frequencies between 50 kHz and 1 MHz along *b* and *c* axes of the monoclinic system for $[C_3H_5N_2]_3[Sb_2Br_9]$ upon first cooling.

It was found that the dielectric response for the form I is well described by the Cole–Cole relation:

$$\varepsilon^*(\omega) = \varepsilon_\infty + \frac{\varepsilon_0 - \varepsilon_\infty}{1 + (i\omega\tau)^{1-\alpha}}, \quad (1)$$

where ε_0 and ε_∞ are the low and high frequency limits of the electric permittivity, respectively, ω is angular frequency, τ is the macroscopic relaxation time. The Cole–Cole diagrams at selected temperatures (within 100 and 122 K) are presented in Fig. 5. The Cole–Cole plots deviate from semi-circles and α ranges between 0.17 and 0.37 units. It means that over this temperature region we deal with a clear polydispersive relaxation process. The distribution of the relaxation times can be explained in terms of the motion of non-equivalent imidazolium cations.

We have fitted the experimental Cole–Cole plots taken at several temperatures with Eq. (1) and determined the fitting parameters ε_0, ε_∞, and τ. A significant slowing down of the macroscopic relaxation time τ (from 3.4×10^{-7} to 1.3×10^{-5} s) is observed for the interval 23 K (see Fig. 6). For the systems with the relatively small dipole–dipole interactions we can assume that the macroscopic relaxation time is equivalent to the microscopic one. Thus, the energy barrier E_a was estimated from the Arrhenius relation for the macroscopic relaxation

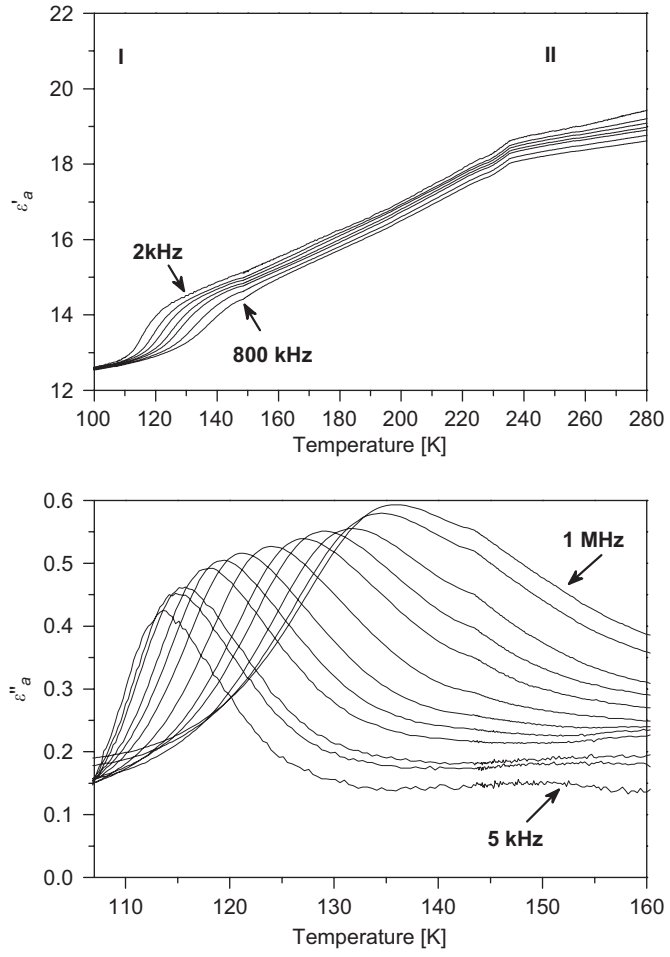

Fig. 4. Frequency dependencies of ε'_a and ε''_a at various temperatures for the low temperature form I of $[C_3H_5N_2]_3[Sb_2Br_9]$.

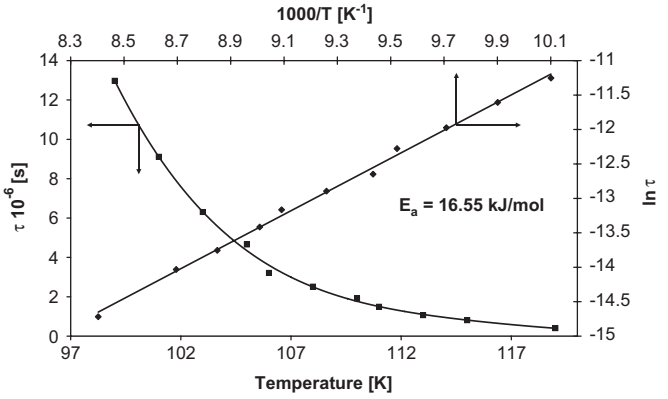

Fig. 6. Temperature dependence of τ vs temperature and ln τ vs reciprocal temperature obtained from the Cole–Cole formula over the form I of $[C_3H_5N_2]_3[Sb_2Br_9]$.

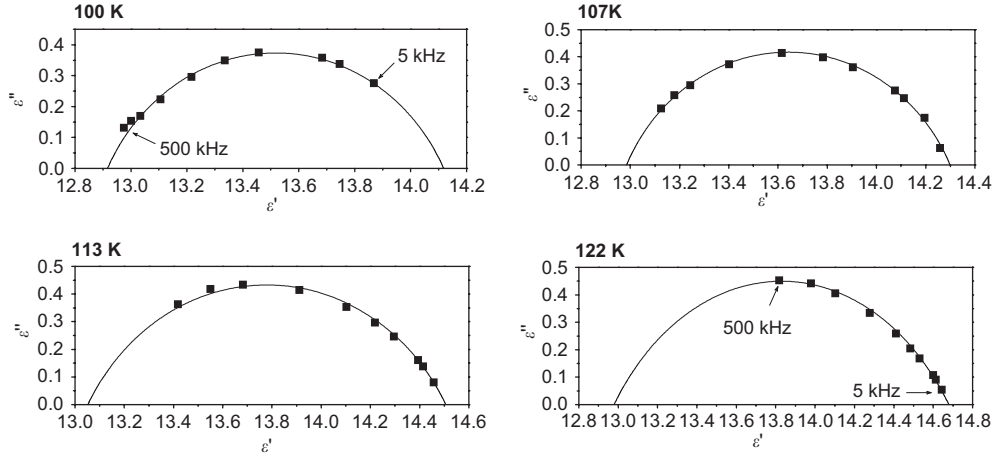

Fig. 5. Cole–Cole plots of ε'' vs ε' (the *a*-axis) at four selected temperatures for the low temperature form I showing a relaxation nature of the dielectric dispersion in $[C_3H_5N_2]_3[Sb_2Br_9]$.

time:

$$\tau = C\exp\left(\frac{E_a}{kT}\right). \quad (2)$$

E_a was estimated to be ca. 16.5 kJ/mol (see Fig. 6).

3.3. Single crystals X-ray analysis

Since the $[C_3H_5N_2]_3[Sb_2Br_9]$ crystal undergoes reversible structural phase transition at 237 K to explain its mechanism, we decided to characterize the structure in two various phases. The crystal structure of the $[C_3H_5N_2]_3[Sb_2Br_9]$ compound was determined at 100 and 293 K. Both forms were solved in the same monoclinic space group no. 14, but in different settings, $P2_1/c$ and $P2_1/n$, respectively. In Fig. 7 independent parts of I and II are shown. The labeling of the atoms was constructed in such a way, that label of each bromine atom in the room-temperature form consists of the numbers that correspond to the labels of two bromine atoms from the lower-temperature form, that

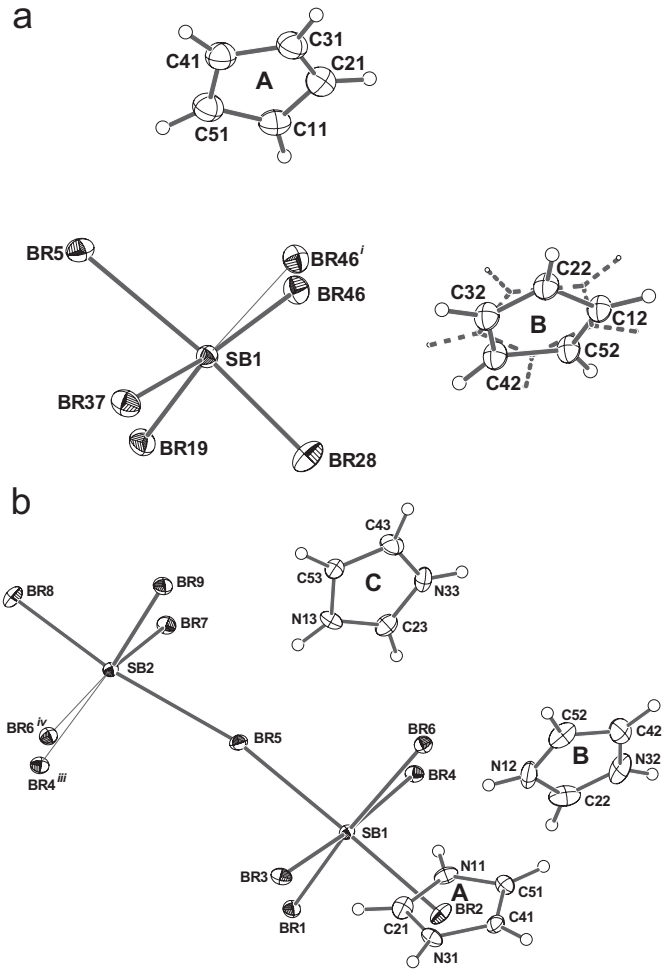

Fig. 7. (a) The asymmetric unit of $[C_3H_5N_2]_3[Sb_2Br_9]$ at 293 K (form II) and (b) at 100 K (form I) showing the atom numbering scheme with bold bonds. Displacement ellipsoids are shown at the 20% and 45%, respectively. Symmetry codes are given in Table 2. Two positions of three disordered cations in form II are shown with solid and dashed lines.

appear due to the loss of the half of the centers of symmetry and 2_1 axes during the phase transition (except for the Br5 atom, which lies on the center of symmetry). Asymmetric unit of form I contains two antimony atoms (Sb1 and Sb2) and nine independent bromine atoms, which are depicted in Fig. 7(b) as connected with the metal atoms by bold bonds. In the unit cell of I one can distinguish three non-equivalent imidazolium cations, which turned to be fully ordered. Cations of A and C type lie below Sb2 and above Sb1 octahedra, respectively. Cations of B type occupy the 12-membered vacancies in the anionic layer. The independent part of II unit cell is twice reduced in comparison to the one of I ($(C_3N_2H_5)_{1.5}SbBr_{4.5}$) vs ($(C_3N_2H_5)_3Sb_2Br_9$). Asymmetric unit of form II consists of one antimony atom surrounded by five independent bromine atoms, of which Br5 lies on the center of inversion. As one can see in Fig. 7(a) there are two independent imidazolium cations (types A and B). Cations of type A correspond to A and C types of form I. They were expected to be ordered, but a more precise examination revealed a disorder of the rotation type. The fact that we could not distinguish the definite nitrogen atoms positions, as well as the significant atom displacement parameters of all the imidazole ring atoms allows to claim that rotational disorder takes place at this temperature. We can expect that cations of type A perform the reorientation within the plane of the imidazole ring. Cations of type B are evidently disordered being equally distributed over two sites, related by a center of symmetry. The positions of nitrogen atoms for this cation also could not be distinguished. For both types of imidazolium cations all atom positions were refined as carbon atoms.

The crystal structure of the two studied forms of $[C_3H_5N_2]_3[Sb_2Br_9]$(form I at 100 K and form II at 293 K) are built up from two-dimensional inorganic fragments of $[Sb_2Br_9^{3-}]$ composition. Antimony atoms have distorted octahedral environment, Sb–Br distances fall into two ranges: ~2.6 and ~3.1 Å for terminal and bridging halogen atoms, respectively (see Table 2). Fig. 8 is relative to the low temperature form. From this figure it is seen that each $[SbBr_6]$ octahedron is connected *via* three of six vertices with adjacent ones giving rise to the (6, 3) hexagonal net that has been already observed in several compounds with ferroelectric properties [24]. Two types of these octahedra are present in the crystal structure: half lay below (Sb1) and another half above (Sb2) the average net plane. Thus, this net forms the corrugated two-dimensional layer (Fig. 9) with the cations of type B placed in the vacancies of the net. All cation moieties positions are stabilized additionally by hydrogen bonds of N–H...Br type (see Table 3) and rather weak C–H...Br contacts. No $\pi-\pi$ stacking between cations is observed.

To clarify the molecular mechanism of the phase transition in $[C_3H_5N_2]_3[Sb_2Br_9]$ we should consider in detail the structural changes accompanying this transformation. Continuous phase transition at 237 K is suggested to be of order-disorder type. The volume of the I cell is

Table 2
Selected bond lengths (Å) and angels (°) for II and I

Form II		Form I			
Sb1–Br19	2.603(2)	Sb1–Br1	2.609(1)	Sb2–Br9	2.606(1)
Sb1–Br37	2.612(2)	Sb1–Br3	2.643(1)	Sb2–Br7	2.595(1)
Sb1–Br28	2.621(2)	Sb1–Br2	2.643(1)	Sb2–Br8	2.589(1)
Sb1–Br5	3.086(1)	Sb1–Br5	3.018(1)	Sb2–Br5	3.136(1)
Sb1–Br46	3.130(2)	Sb1–Br4	3.037(1)	Sb2−Br4^{iii}	3.129(1)
Sb1−Br46^{i}	3.156(2)	Sb1–Br6	3.131(1)	Sb2−Br5^{iv}	3.205(1)
Br19–Sb1–Br37	92.47(8)	Br1–Sb1–Br3	92.63(4)	Br7–Sb2–Br9	93.11(4)
Br19–Sb1–Br28	90.34(8)	Br1–Sb1–Br2	90.19(3)	Br8–Sb2–Br9	90.42(3)
Br37–Sb1–Br28	92.77(8)	Br2–Sb1–Br3	94.33(3)	Br8–Sb2–Br7	92.87(3)
Br19–Sb1–Br5	84.66(6)	Br1–Sb1–Br5	86.43(3)	Br9–Sb2–Br5	83.56(3)
Br37–Sb1–Br5	85.91(6)	Br3–Sb1–Br5	87.90(3)	Br7–Sb2–Br5	83.97(3)
Br28–Sb1–Br5	174.76(7)	Br2–Sb1–Br5	176.04(3)	Br8–Sb2–Br5	173.02(3)
Br19–Sb1–Br46	88.22(7)	Br1–Sb1–Br4	87.54(4)	Br9−Sb2−Br6^{iv}	89.28(4)
Br37–Sb1–Br46	175.59(7)	Br3–Sb1–Br4	175.69(3)	Br7−Sb2−Br6^{iv}	174.88(3)
Br28–Sb1–Br46	91.58(7)	Br2–Sb1–Br4	89.98(3)	Br8−Sb2−Br6^{iv}	91.64(3)
Br5–Sb1–Br46	89.82(5)	Br5–Sb1–Br4	87.81(3)	Br5−Sb2−Br6^{iv}	91.81(2)
Br19−Sb1−Br46^{i}	176.03(6)	Br1–Sb1–Br6	175.47(3)	Br9−Sb2−Br4^{iii}	176.34(3)
Br37−Sb1−Br46^{i}	89.10(7)	Br3–Sb1–Br6	89.85(4)	Br7−Sb2−Br4^{iii}	88.11(4)
Br28−Sb1−Br46^{i}	85.94(7)	Br2–Sb1–Br6	85.85(3)	Br8−Sb2−Br4^{iii}	86.08(3)
Br5−Sb1−Br46^{i}	99.10(5)	Br5–Sb1–Br6	97.45(3)	Br4^{iii}−Sb2−Br5	100.00(3)
Br46−Sb1−Br46^{i}	90.50(4)	Br4–Sb1–Br6	90.27(3)	Br4^{iii}−Sb2−Br6^{iv}	89.77(3)
Sb1−Br5−Sb1^{ii}	180	Sb1–Br5–Sb2	169.75(3)		

Symmetry codes for form II: (i) $\frac{3}{2}-x, \frac{1}{2}+y, \frac{1}{2}-z$; (ii) $2-x, 2-y, 1-z$.
Symmetry codes for form I: (iii) $x, -\frac{1}{2}-y, z-\frac{1}{2}$; (iv) $x, \frac{1}{2}-y, z-\frac{1}{2}$.

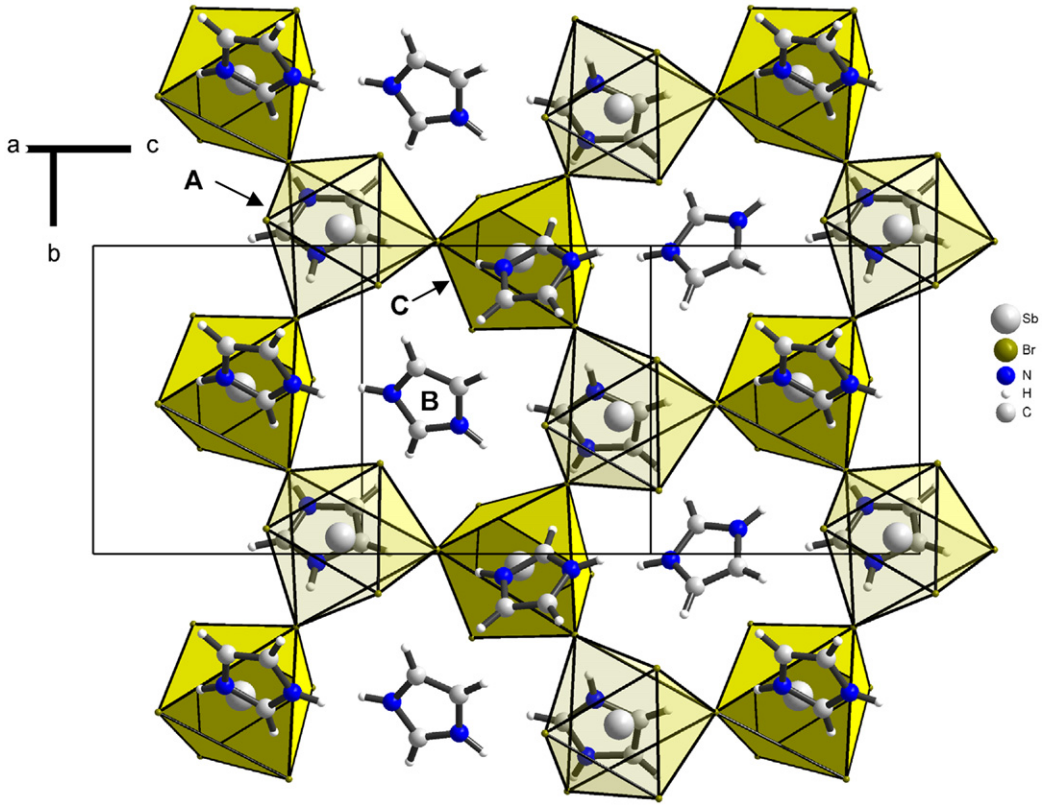

Fig. 8. Projection of the crystal structure of $[C_3H_5N_2]_3[Sb_2Br_9]$ at 100 K (I) on the *cb* plane as a polyhedral representation. Sb2 octahedra are made transparent to show A type cations.

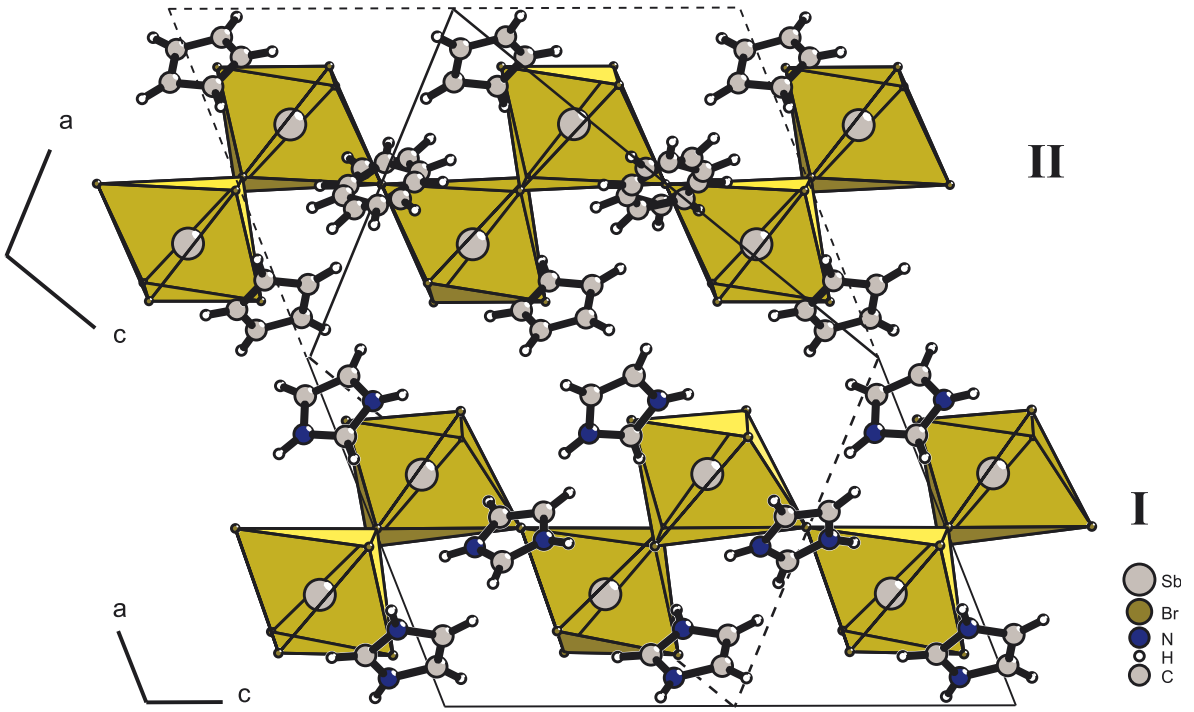

Fig. 9. Projection of the crystal structure packing of $[C_3H_5N_2]_3[Sb_2Br_9]$, viewed down the *b*-axis, showing inorganic layer sublattice along with imidazolium cations. Forms I (bottom) and II (top) are shown with mutually overlaid unit cells, depicted as broken lines.

Table 3
Hydrogen bonds for $[C_3H_5N_2]_3[Sb_2Br_9]$ (Å) and (deg) at 100 K (form I)

D–H...A	D–H	H...A	D...A	<(DHA)
N11–H11...Br6	0.88	2.58	3.388(6)	154
N31–H31...Br3^{v}	0.88	2.66	3.437(6)	147
N12–H12...Br6	0.88	2.85	3.497(7)	132
N12–H12...Br2	0.88	3.11	3.785(8)	135
N32–H32...Br4^{vi}	0.88	2.63	3.493(7)	165
N13–H13...Br5	0.88	2.48	3.315(7)	158
N33–H33...Br7^{vi}	0.88	2.85	3.504(7)	133

Symmetry codes: (v) $-x, y+\frac{1}{2}, \frac{1}{2}-z$; (vi) $x, -y-\frac{1}{2}, z+\frac{1}{2}$.

twice as big as the II one. Both I and II crystallize in the same type of monoclinic space group, but in different settings: $P2_1/c$ and $P2_1/n$, respectively. The phase transition from I to II is associated with the appearance of additional centres of symmetry and 2_1 screw axes (Fig. 10). The *c*-glide plane changes only its designation to *n*, due to the changed *a* and *c* axes directions. The relation between the cells is described by following matrices: $\frac{1}{2}, 0, \frac{1}{2}; 0, 1, 0; -\frac{1}{2}, 0, \frac{1}{2}$ (I cell → II cell), 1, 0, −1; 0, 1, 0; 1, 0, 1 (II cell → I cell).

The observed 2_1 screw axes in form II connect the Sb1 and Sb2 octahedra, the Br5 atom lies on a special position on the inversion center. The arising centers of symmetry connect the A and C cations and two disordered positions of the B cation. The change in the diffraction pattern during the I → II phase transition is associated with the

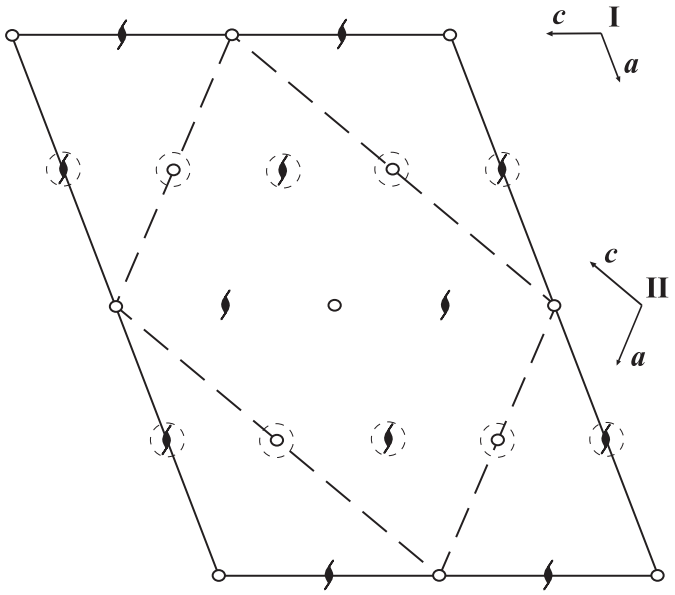

Fig. 10. View of the symmetry elements in the cell I and II along the *b*-axis. Symmetry elements which disappear during the II → I phase transition are depicted in dotted circles.

double reduction of the reflections number, where all reflections with odd $h+l$ (I form) disappear. It should be noted that during the II → I phase transition the additional centres of symmetry and the 2_1 screw axes do not disappear completely, they remain as pseudoelements of symmetry. The reflections with odd $h+l$ (I form) are weaker than the remaining ones. It is consistent with the

fact that the only considerable structural change during the phase transition is concerned with disorder of the B cations. The geometry of the inorganic sublattice remains practically unchanged, resulting mainly from the hydrogen-bonds network rearrangement.

The temperature dependencies of the lattice parameters a, b, c, β and the volume of the unit cell over the temperature range 110–270 K are shown in Fig. 11. One anomaly of the lattice parameters is observed close to 235 K (±2 K) which corresponds to the structural phase transition disclosed by DSC measurements. The best shape structural anomaly appears along the c-axis, unexpectedly characterizing even discontinuous transitions. Values of the lattice parameters along all directions decrease significantly with the temperature decreasing which justifies an important reduction in the mobility of dipolar cationic moieties. The monoclinic β angle experiences the value decrease by nearly 0.7° below 235 K, which reflects a distortion of the unit cell over the I form. The volume of the unit cell can be well approximated over the wide temperature region by a straight line, except for the vicinity of the II → I phase transition. The values of the dV/dT are different over the II and I forms being significantly larger for the II form.

4. Discussion

The title compound is characterized by a two-dimensional polymeric layer formed by ($Sb_2Br_9^{3-}$) moieties. In the room-temperature structure one can distinguish two types of imidazolium cations (the ratio 2:1). The cations of type A placed between the layers are characterized by large thermal displacement parameters. The cations of type B, which occupy the 12-membered rings inside the layers were

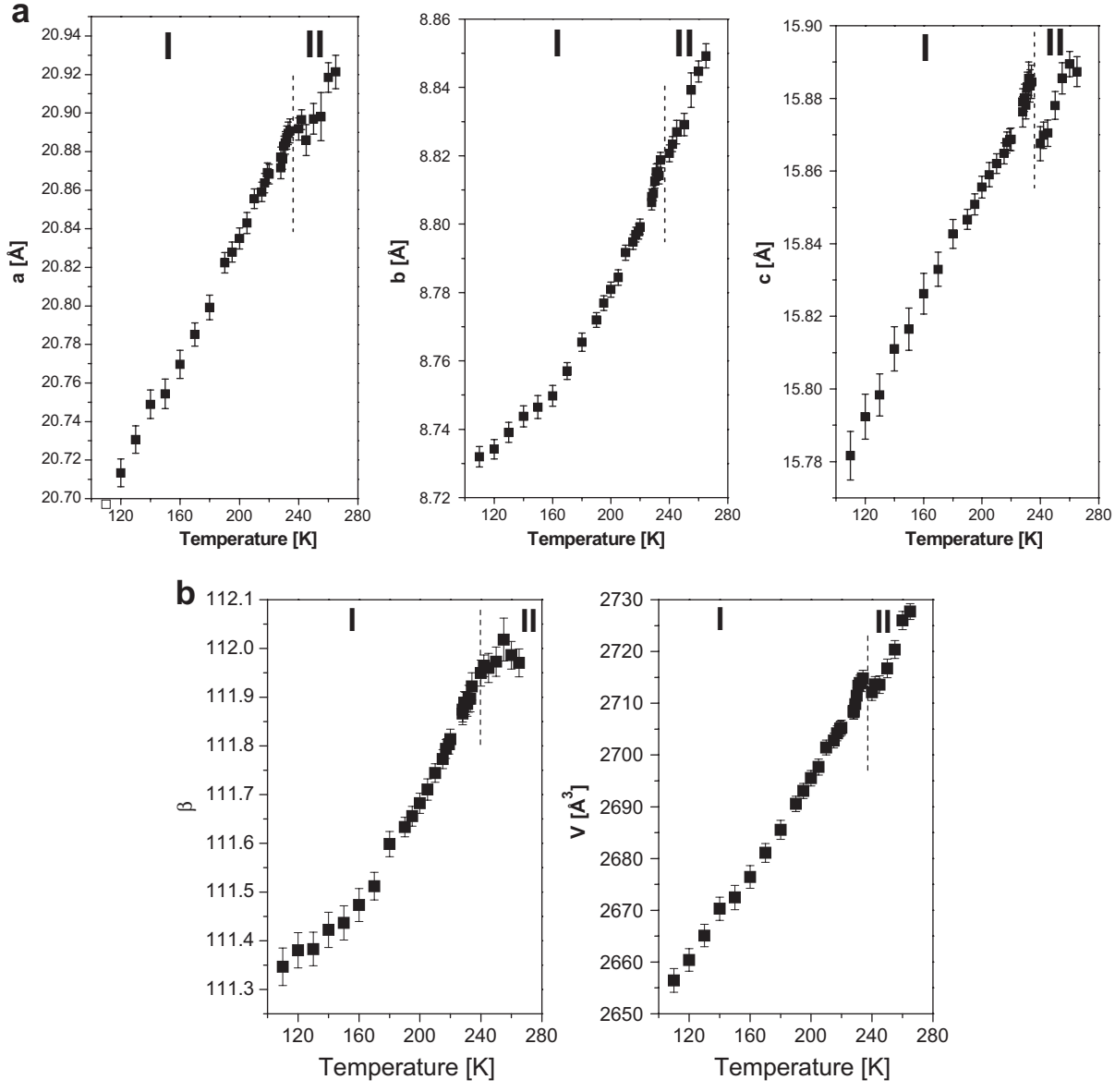

Fig. 11. Temperature dependencies of (a) the a, b and c lattice constants and (b) the monoclinic β angle and volume of unit cell.

Table 4
The phase transitions sequence in $R_3M_2X_9$ type ferroelectrics: monoclinic β angle for the ferroelectric ordered phase (P_c) for dimethyl- and trimethyl-ammonium analogs, P_s—saturated spontaneous polarization

Compounds	Sequence of phase transitions			Ref.
$(CH_3NH_3)_3Sb_2Br_9$	Paraelastic($P\bar{3}m1$) → ferroelastic($C2/m$) → ferroelectric (point group 2)			[21]
$(CH_3NH_3)_3Bi_2Br_9$	Paraelastic($P\bar{3}m1$) → ferroelastic($C2/m$) → ferroelastic(?)⟶ferroelastic(2)			[22,23]
		β (°)	$Ps(10^{-2}\,C\,m^{-2})$	
$[(CH_3)_2NH_2)]_3Sb_2Br_9$	Ferroelastic($P2_1/c$) → ferroelectric(P_c)	95.10	0.70	[24]
$[(CH_3)_2NH_2)]_3Sb_2Cl_9$	Ferroelastic($P2_1/c$) → ferroelectric(P_c)	95.81	0.69	[4]
$[(CH_3)_3NH)]_3Sb_2Cl_9$	Ferroelastic($P2_1/c$) → ferroelectric(P_c)	89.82	3.0	[5,25]

found to be highly disordered, being distributed over two equally occupated positions (two-sites model). It should be underlined that the structural situation resembles those encountered in numerous ferroelectric materials crystallizing with $R_3M_2X_9$ composition and characterized by two-dimensional layers. However, in spite of these structural similarities, the sequence of phase transitions and physical properties of crystals are different. Table 4 illustrates the phase situation in various $R_3M_2X_9$ salts exhibiting ferroic properties.

No structural results are available for the low temperature ferroelectric phase (form) of the methylammonium analogs. The diagram data reveal that the title compound, may be isomorphic in some disordered forms. However, in the case of $[C_3H_5N_2]_3[Sb_2Br_9]$ the space group $P2_1/c$ verifies the fully ordered form (I), whereas in the case of all analyzed ferroelectrics the $P2_1/c$ space group is characteristic for their disordered or partially disordered forms. It implies different dynamics within the cations sublattice in the title crystal and the mentioned ferroelectrics. However, all analyzed compounds possess a common feature—a high disorder of organic cations in their high temperature forms. The methylammonium analogs are characterized by an isotropic rotation of cations in the room-temperature form ($P\bar{3}m1$). The disorder of the dimethylammonium and trimethylammonium cations in the paraelectric form is more restricted. The dimethylammonium cations were found to be distributed over two sites. The imidazolium cations are expected to show a similar disorder (two-sites model), however, their mobility is the lowest. It may be related to the fact that the $C_3H_5N_2^+$ cations possess two donor protons, which form the expanded system of the hydrogen bonds stiffening dipolar organic units in the lattice. In comparing of the dynamical abilities of the cations it should be also taken into account that the shape and the size of imidazolium cations differ from monomethyl-, dimethyl- and trimethyl-ammonium ones. The latter are rather small and can reorient freely in the vacancies of the inorganic sublattice, meanwhile the former are able to reorient only within the plane of the imidazole ring.

It is obvious, that the origin of ferroelectricity in the $R_3M_2X_9$ compounds with monomethyl-, dimethyl- and trimethyl-ammonium cations is strictly connected with the dynamics of organic cations in the vacancies provided by a two-dimensional inorganic sublattice. Though being so similar to the ones with monomethyl-, dimethyl- and trimethyl-ammonium derivatives, the title compound possesses no ferroelectric properties. This phenomenon is conditioned by the inorganic sublattice arrangement. The room-temperature form II of $[C_3H_5N_2]_3[Sb_2Br_9]$ was expected to be isomorphic with the paraelectric $P2_1/c$ form of dimethyl- and trimethyl-ammonium analogs. But this form cannot be treated as the isomorphic one on account of a significant difference in the monoclinic β angle. The monoclinic β angle is the measure of the shift of adjacent inorganic layers. In the case of monomethyl-, dimethyl- and trimethyl-ammonium salts the β value is close to 90°, thus the inorganic layers are stacked with a moderate shift giving rise to channels occupied by organic cations (cf. Fig. 9). Such arrangement enables a long-range ordering of dipolar cations in the ferroelectric form. In the case of the compound under consideration the inorganic layers are mutually shifted, so that below and above each vacancy of the 12-membered net one can find the $[SbBr_6]$ octahedra of adjacent inorganic fragments. In our opinion this process screens dipolar interactions between organic cations and hinders a long-range ordering, required for the ferroelectric phase occurrence. This explanation seems to be consistent with the structural results reported for the dimethyl- and trimethyl-ammonium analogs (see Table 4). The $[(CH_3)_3NH]_3Sb_2Cl_9$ crystal is characterized by the closest to 90° angle and the largest value of P_s ($3.0\times10^{-2}\,C/m^2$) among three $R_3M_2X_9$ ferroelectrics. With an increase of the monoclinic β angle the spontaneous polarization (directly connected with the strength of dipolar interactions) decreases. This result leads to the conclusion that the mutual shifting of parallel inorganic layers, reflected in the monoclinic angle, is one of the most important factors, which determines the possibility of generation of ferroelectricity in the two-dimensional $R_3M_2X_9$ ferroelectrics.

5. Conclusion

In this paper we have reported the structural characterization of $[C_3H_5N_2]_3[Sb_2Br_9]$ in its various forms at 100 and 293 K based on single-crystal X-ray diffraction data. The crystal structure consisting of corrugated layer formed by $[Sb_2Br_9]^{3-}$ and disordered imidazolium cations

at room-temperature resembles to a high extent those encountered in $R_3M_2X_9$—type ferroelectrics. Despite of large structural similarities no ferroelectric properties are disclosed in $[C_3H_5N_2]_3[Sb_2Br_9]$. It may be explained in terms of a significant distortion of the polymeric anionic sublattice, expressed by a large monoclinic β angle, which prevents the dipole–dipole interactions responsible for the ferroelectric order in low temperature form. The title compound was found to undergo the structural phase transition at 237 K from $P2_1/n$ to $P2_1/c$ monoclinic space group, which is due to the dynamics of $C_3H_5N_2^+$ moieties. The motion of dipolar organic cations over the lowest temperature form (I) is directly reflected in the presence of a low frequency dielectric relaxation process.

Acknowledgment

This work was supported by the Polish State Committee for Scientific Research (Project Register No. N204 108 31/2551).

Appendix A. Supplementary material

Crystallographic data (excluding structure factors) for the structure reported in this paper have been deposited with the Cambridge Crystallographic Data Center as supplementary publication nos. CCDC-613438, −613439. Copies of the data can be obtained free of charge on application to CCDC, 12 Union Road, Cambridge CB2 1EZ, UK (fax: 44 1223 336 033; E-mail: deposit@ccdc.cam.ac.uk).

References

[1] R. Jakubas, L. Sobczyk, Phase Transitions 20 (1990) 163–193.
[2] L. Sobczyk, R. Jakubas, J. Zaleski, Pol. J. Chem. 71 (1997) 265–300 (and references cited therein).
[3] M. Hall, M. Nunn, M. J. Begley, D.B. Sowerby, J. Chem. Soc., Dalton Trans. (1986) 1231–1238.
[4] J. Zaleski, A. Pietraszko, Acta Crystallogr. B 52 (1996) 287–295.
[5] A. Kallel, J. Bats, Acta Crystallogr. C41 (1985) 1022–1024.
[6] P. Carpentier, J. Lefebvre, R. Jakubas, Acta Crystallogr., Sect. B 51 (1995) 167–174.
[7] J. Jóźków, G. Bator, R. Jakubas, A. Pietraszko, J. Chem. Phys. 114 (2001) 7239–7246.
[8] K. Matyjasek, J. Phys. D 33 (2000) 2553–2559.
[9] K. Matyjasek, R.Z. Rogowski, J. Appl. Phys. 99 (2006) 074107, 1–7.
[10] M.H. Kuok, S.G. Ng, L.S. Tan, Z.L. Rang, M. Iwata, Y. Ishibashi, Solid State Commun. 108 (1998) 159–163.
[11] M. Iwata, M. Eguchi, Y. Ishibashi, S. Sasaki, H. Shimizu, T. Kawai, S. Shimanuki, J. Phys. Soc. Jpn. 62 (1993) 3315–3326.
[12] Y. Iwata, N. Koyano, M. Machida, M. Iwata, Y. Ishibashi, Ferroelectrics 237 (2000) 229–236.
[13] T. Kawai, E. Takao, S. Shimanuki, M. Iwata, A. Miyashita, Y. Ishibashi, J. Phys. Soc. Jpn. 68 (1999) 2848–2856.
[14] R. Jakubas, Z. Czapla, Z. Galewski, L. Sobczyk, O.J. Żogal, T. Lis, Phys. Stat. Sol. (a) 93 (1986) 449–455.
[15] B. Aurivillius, C. Stälhandske, Acta Chem. Scand. A 32 (1978) 715–719.
[16] A. Piecha, R. Jakubas, A. Pietraszko, J. Baran, J. Mol. Struct., (2006), doi:10.1016/j.molstr.2006.06.017.
[17] R. Jakubas, A. Piecha, A. Pietraszko, G. Bator, Phys. Rev. B 72 (2005) 104107–104114.
[18] *CrysAlis RED*, ver. 1.171, Oxford Diffraction Poland, 1995–2003.
[19] R.C. Clark, J.S. Reid, Acta Crystallogr. A 51 (1995) 887–897.
[20] G. M. Sheldrick, *SHELX*. Program for the Solution and Refinement of Crystal Structures, University of Göttingen, Germany, 1997.
[21] R. Jakubas, Z. Galewski, L. Sobczyk, J. Matuszewski, J. Phys. C Solid State Phys. 18 (1985) L857–L860.
[22] T. Umeki, H. Kasatani, H. Terauchi, M. Iwata, Y. Ishibashi, Trans. Mater. Res. Soc. Jpn. 14B (1994) 1743–1746.
[23] M. Iwata, Y. Ishibashi, Ferroelectrics 135 (1992) 283–289.
[24] J. Zaleski, Cz. Pawlaczyk, R. Jakubas, H.-G. Unruh, J. Phys. Condens. Matter 12 (2000) 7509–7521.
[25] M. Bujak, J. Zaleski, Cryst. Eng. 4 (2001) 241–252.